Lawrence Berkeley National Laboratory

Title

Observing cosmic-ray extensive air showers with a silicon imaging detector.

Permalink

https://escholarship.org/uc/item/2637g745

Journal

Scientific Reports, 13(1)

Authors

Kawanomoto, Satoshi
Koike, Michitaro
Bradfield, Fraser
et al.

Publication Date

2023-10-12

DOI

10.1038/s41598-023-42164-4

Peer reviewed

scientific reports

OPEN

Observing cosmic-ray extensive air showers with a silicon imaging detector

Satoshi Kawanomoto[1]✉, Michitaro Koike[1]✉, Fraser Bradfield[2], Toshihiro Fujii[2,3]✉, Yutaka Komiyama[4], Satoshi Miyazaki[5,6], Tomoki Morokuma[7], Hitoshi Murayama[8,9,10], Masamune Oguri[11,12] & Tsuyoshi Terai[5]

Extensive air showers induced from high-energy cosmic rays provide a window into understanding the most energetic phenomena in the universe. We present a new method for observing these showers using the silicon imaging detector Subaru Hyper Suprime-Cam (HSC). This method has the advantage of being able to measure individual secondary particles. When paired with a surface detector array, silicon imaging detectors like Subaru HSC will be useful for studying the properties of extensive air showers in detail. The following report outlines the first results of observing extensive air showers with Subaru HSC. The potential for reconstructing the incident direction of primary cosmic rays is demonstrated and possible interdisciplinary applications are discussed.

Cosmic-ray extensive air showers and surface detector arrays

Cosmic rays are energetic particles from the universe discovered by V. F. Hess[1]. Their origin, acceleration mechanisms and mass composition at the highest energies are still largely unknown. In particular, determining the origin of high-energy cosmic rays is considered to be among the most important problems in modern astrophysics[2,3]. The flux of cosmic rays arriving at Earth follows a power-law function of roughly E^{-3}, where E is the primary energy of the cosmic rays. As such, high-energy cosmic rays are extremely rare and are typically studied indirectly. This is accomplished by measuring the showers of secondary particles produced when primary cosmic rays interact with atmospheric nuclei, called "extensive air showers" (EASs).

Several methods are used to observe EASs, such as the detection of fluorescence light[4,5] and radio emission[6–8] from the electromagnetic component of an EAS. Another method is the use of surface detector (SD) arrays—collections of ground based particle detectors spread across several hundreds or thousands of square kilometers[5,9,10]. Such arrays measure the arrival times and densities of the secondary particles from an EAS at ground level. This information is used to reconstruct the arrival direction, primary energy and mass composition information of the initial cosmic ray. As an example, the Telescope Array experiment in Utah, USA, uses 507 plastic scintillators, deployed with a spacing of 1.2 km, to form a detecting area of ~700 km^2 to cosmic rays with energies above 10^{19} eV[9]. By combining measurements from several detectors, the energy and arrival direction of the primary cosmic ray are determined. However, as is typical for surface detectors, these scintillators are unable to measure the properties of individual secondary particles during normal operation. Such information would be useful for identifying the primary particle and studying high-energy particle interactions[11,12].

[1]National Astronomical Observatory of Japan, Osawa, Mitaka, Tokyo 181-8588, Japan. [2]Graduate School of Science, Osaka Metropolitan University, Sumiyoshi, Osaka 558-8585, Japan. [3]Nambu Yoichiro Institute of Theoretical and Experimental Physics, Osaka Metropolitan University, Sumiyoshi, Osaka 558-8585, Japan. [4]Department of Advanced Sciences, Faculty of Science and Engineering, Hosei University, Kajino-cho, Koganei, Tokyo 184-8584, Japan. [5]Subaru Telescope, National Astronomical Observatory of Japan, Hilo, HI 96720, USA. [6]SOKENDAI, Graduate University for Advanced Studies, Osawa, Mitaka, Tokyo 181-8588, Japan. [7]Planetary Exploration Research Center, Chiba Institute of Technology, Tsudanuma, Narashino, Chiba 275-0016, Japan. [8]Berkeley Center for Theoretical Physics, University of California, Berkeley, CA 94720, USA. [9]Theory Group, Lawrence Berkeley National Laboratory, Berkeley, CA 94720, USA. [10]Kavli Institute for the Physics and Mathematics of the Universe (WPI), University of Tokyo, Kashiwa, Chiba 277-8583, Japan. [11]Center for Frontier Science, Chiba University, Inage, Chiba 263-8522, Japan. [12]Department of Physics, Graduate School of Science, Chiba University, Inage, Chiba 263-8522, Japan. ✉email: kawanomoto.satoshi@nao.ac.jp; michitaro.koike@nao.ac.jp; toshi@omu.ac.jp

To this end, this paper details the first results of utilizing the world-class silicon imaging detector Subaru Hyper Suprime-Cam to observe individual tracks of EAS particles with unprecedented statistics and precision. In doing so, we develop a new method of observing EASs.

Observing extensive air showers with Subaru Hyper Suprime-Cam

Subaru Hyper Suprime-Cam (HSC)[13] is the prime-focus wide field camera on Subaru Telescope. Located atop Maunakea in Hawaii, it is the largest silicon imaging detector above an altitude of 4200 m. Subaru HSC typically observes distant stars, galaxies and other interstellar objects in the optical and infrared. This is achieved by employing 112 Charge Coupled Devices (CCDs) each with dimensions of 4176×2048 pixels. Of these 112 CCDs, 104 are used for scientific observation and the remaining 8 are for calibration. The total area of the CCDs which perform observations is 0.196 m^2.

Standard operation of Subaru HSC involves taking images or "exposures" of targets of interest throughout a night. Typical exposure times for individual images are 150 or 200 seconds. During an exposure charged particles from the atmosphere may penetrate into the depletion layer of the CCDs. These particles leave long, thin "tracks" on the final image where the length of a track indicates the particle's angle of entry into the CCD. Normally, these tracks are sparse and randomly directed, and so are treated as unwanted noise which is removed. However, during the standard analysis of the Subaru HSC data, we encountered several images which displayed a far larger number of tracks than usual. Moreover, within each of these images, the majority of the tracks were aligned in a similar direction and were of similar lengths, indicating that the particles were travelling with similar trajectories. In turn we concluded that, for each of these images, the bulk of the detected particles had originated from a single, high-energy cosmic ray induced, EAS. We wish to emphasize the fact that the observation of these EASs was fortuitous and simply occurred during the normal operation of Subaru HSC. An example of one such image is shown in Fig. 1.

Figure 1 contains several particle tracks not aligned with the general direction of the shower. These may be deflected particles from the same shower, or randomly directed particles originating from the constant background of low energy cosmic ray showers. Understanding the background rate of these randomly directed particles is important as, based on how we initially found EAS events in our data, we expect the number of particle tracks in an image where an EAS was present to be significantly greater than the background rate. Thus, by comparing the expected number of "background tracks" in an image to the measured number, we can determine which exposures have observed an EAS. To achieve this, the following section constructs a model to describe the number of background tracks expected to be observed by Subaru HSC in different operating conditions.

Before continuing, it is important to note that with only one silicon imaging detector, as is the case with our current data, it is not possible to determine the energy, arrival direction or mass composition information of the original cosmic rays. However, with additional detectors spaced in a similar fashion to a regular SD array, these properties could in principle be reconstructed. Additionally, we expect that the detailed measurements of individual secondary particles by silicon imaging detectors could be used in conjunction with standard SD arrays as an effective method for studying EASs in detail. Both of these points are discussed further in Section "Discussion and future objectives".

Figure 1. An example of a cosmic-ray extensive air shower recorded by a CCD of Subaru HSC. Dimensions: 4176 × 2048 pixels = 62.6 mm × 30.7 mm. The high density of aligned tracks, indicative of an EAS, is clearly visible in the upper right portion of the image.

Modeling the background rate of secondary particles

To effectively search for EASs among Subaru HSC data, it is necessary to formulate a model for the number of randomly directed, background electromagnetic and muonic particles expected to leave tracks on a Subaru HSC image, given various data-taking conditions. We label this value N_{model}. The various contributions to N_{model} are described below, where the telescope elevation angle, telescope azimuth angle and sky brightness level are given by ψ_{tel}, ϕ_{tel}, and B_{sky} respectively. Zero degrees azimuth was defined to be south, with azimuth increasing clockwise.

Effective area

We expect the number of detected tracks to be proportional to the effective detection area of the CCDs. This area itself is proportional to the absolute value of the cosine of angular separation between the telescope pointing direction and incoming cosmic ray direction. Given the cosmic ray azimuth angle, ϕ_{CR}, and cosmic ray zenith angle, θ_{CR}, the cosine of angular separation is given by:

$$\cos\alpha = \cos\theta_{CR}\sin\psi_{tel} + \sin\theta_{CR}\cos\psi_{tel}\cos(\phi_{tel} - \phi_{CR}) \tag{1}$$

where α is angular separation.

Assuming that the zenith angle dependency of the cosmic ray flux at Earth is $\cos^2\theta_{CR}$, the expected cosmic ray flux at telescope elevation ψ_{tel} is proportional to the solid angle integral

$$\int_0^{2\pi}\int_0^{\pi/2} \cos^2\theta_{CR}\,|\cos\alpha|\,\sin\theta_{CR}\,d\theta_{CR}\,d\phi_{CR} = \frac{\pi}{4}(1 + \sin^2\psi_{tel}). \tag{2}$$

Therefore, the term $(1 + \sin^2\psi_{tel})/2$ is included in our model, where the normalization factor of 1/2 has been chosen so that the term becomes unity at $\psi_{tel} = 90°$ (west).

East-west effect

The east-west effect is a suppression of low-energy positive cosmic rays arriving from the east due to the Earth's magnetic field[14–16]. With our definition of azimuth, this effect can be modelled as proportional to the term $\sin(\phi_{tel})$.

Night sky background

We define the night sky background, B_{sky}, to be the median number of ADC counts across the CCD array over the period of an exposure. This value changes with the background photon flux. Empirically, we have observed that higher values of B_{sky} generally result in a larger number of tracks being detected. These additional tracks are believed to be "false" triggers of the track detection algorithm, not actual secondary particles. Since the exact dependence of B_{sky} on the number of detected tracks is unknown, we assume a basic linear relationship in our model.

Adding the above effects, the final parameterisation of N_{model} is

$$N_{model} = c_0 + c_1(1 + \sin^2(\psi_{tel}))/2 + c_2\sin(\phi_{tel}) + c_3 B_{sky} \tag{3}$$

where c_0, c_1, c_2 and c_3 are fitted parameters. Here, c_0 represents an offset to account for the different responses of the various filters used.

To find these parameters, we fit the above function to data collected by Subaru HSC between March 2014 and January 2020. Subaru labels one measurement of the sky with a specific filter and exposure time as a "visit". For this study, visits with an exposure time of either 150 or 200 s were used. Table 1 below summarises the data showing, for each filter, the measurement period, number of visits in each period, exposure time for a single visit, and the corresponding total exposure time (subtotal). Across all filters, this gave approximately 875 h of data.

For each visit, dedicated software was used to count the number of tracks in the image by searching for different morphologies such as a long-straight, worm-like or wedge-like tracks. The tracks were identified based on a series of conditions, primarily considering the pixel intensity relative to the local background and gradient checks against the point spread functions of the astronomical objects in the image. The procedure is described

Filter	Start	End	# of visits	Exposure time [s]	Subtotal time [s]
HSC-g	Sep. 2014	Jan. 2020	2996	150	449400
HSC-r	Sep. 2014	Jul. 2016	1079	150	161850
HSC-r2	Aug. 2016	Jan. 2020	1737	150	260550
HSC-i	Mar. 2014	Nov. 2015	786	200	157200
HSC-i2	Feb. 2016	Jan. 2020	3091	200	618200
HSC-z	Sep. 2014	Jan. 2020	3887	200	777400
HSC-y	Mar. 2014	Jan. 2020	3632	200	726400
Total time					3151000

Table 1. Summary of the Subaru HSC data used to search for cosmic-ray extensive air showers.
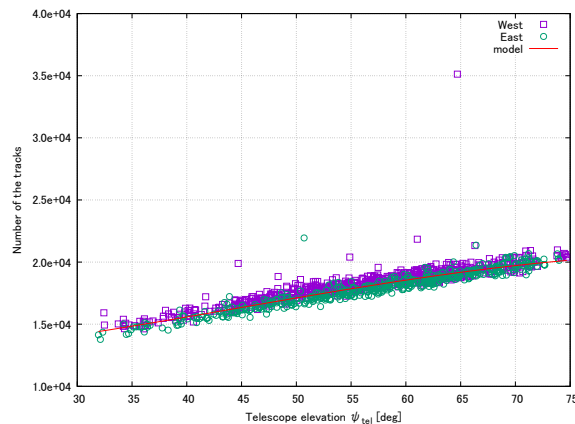
Figure 2. A simplified example of fitting Eq. 3 to track numbers from different visits. The horizontal axis shows the telescope elevation angle. The vertical axis shows the number of detected tracks in a visit. The purple squares and green circles show data that was taken with the telescope pointing west and east respectively. There are several points above the main group of events. These points are likely to be EASs and are removed when applying the 2σ threshold (see text). The red line shows the model fit results, with $\phi_{\text{tel}} = 0°$ and $B_{\text{sky}} = 1000$ counts.

Filter	Material	c_0	c_1	c_2	c_3	σ
HSC-g	Silica	1587±61	17939±69	235±8	0.185±0.027	329
HSC-r	B270	3006±134	17600±146	289±14	0.141±0.027	341
HSC-r2	Silica	1012±84	18437±96	169±11	0.208±0.014	336
HSC-i	B270	8648±287	17819±285	249±28	0.271±0.023	506
HSC-i2	B270	6480±105	19608±109	272±12	0.485±0.009	512
HSC-z	Silica	2865±88	21749±92	272±10	0.494±0.009	448
HSC-y	Silica	6409±126	18614±133	261±14	0.375±0.005	652

Table 2. Results for the parameterisation of N_{model} for each filter.

in depth in Section 4.4 of[17]. Pixels suspected to be contaminated by secondary particles were then grouped into contiguous events and further scrutinized in iterative passes.

Once the number of tracks for each visit had been calculated, the telescope's elevation and azimuthal angles, together with the night sky background levels, were extracted. Equation 3 was then fit to the data from each filter using the following method. Initially, the model was fit to all the data, including events containing EASs, using a χ^2 fit. As the objective was to model the number of *background tracks* we then removed data points with a number of tracks different from the model prediction by 2σ, where σ was the standard deviation of the mean squared errors between the measured data and fitted model. Equation 3 was then fit again to the remaining data and the best fit parameters recorded. We present an example of data and model fitting in Fig. 2.

The parameterisation results for all filters are shown in Table 2 together with σ.

The dependency on elevation angle (c_1) is roughly the same in every filter. Additionally, the azimuthal variation (c_2) shows that the number of cosmic ray tracks from the west is greater than that from the east, as expected from the east-west effect. The values for c_3 are comparatively small as typical values for B_{sky} are on the order of 1000 counts. Finally, we note the large variation in c_0 across the different filters. In particular we see that, despite observing the same optical band, HSC-r has a significantly larger background level than HSC-r2. This may be because B270 contains potassium, a natural radio isotope.

EAS search results

By using the model defined in the previous section, we search for visits in the data-set with a significant excess of tracks compared to our model prediction. For demonstration purposes, we have defined a significant excess to be more than 20σ of each filter. Table 3 shows the significant visits. The telescope elevation angles for these visits, primarily between $50°$ and $70°$, is simply a consequence of those elevations being the most commonly observed.

To determine whether these visits actually observed an EAS, we checked for clustering in the particle arrival directions. Unfortunately, the true 3D trajectories of each particle are impossible to determine with the CCD image alone. This is because there is no method for determining which end of a track corresponds to the top face/bottom face of the CCD. Furthermore, we cannot tell which end corresponds to the particle entering/exiting the CCD. In other words, for a single track there are four possible trajectories, each of which is shown in Fig. 3. If

Visit	Date	UT	Filter	ψ_{tel}	ϕ_{tel}	B_{sky}	N_{track}	N_{model}	N_{excess}
034298	2015-07-14	09:17:32	HSC-g	54.2	138.9	413	24745	16685	8060
034480	2015-07-14	13:28:20	HSC-g	72.7	1.4	423	28276	18760	9516
034814	2015-07-15	14:47:34	HSC-r	64.7	45.5	1559	35124	19424	15700
039340	2015-10-06	14:08:04	HSC-y	43.3	63.4	6209	36354	22328	14026
069450	2016-04-15	10:55:54	HSC-y	55.5	54.3	7843	38513	24810	13703
073808	2016-06-11	09:42:43	HSC-i2	59.0	57.1	2880	99476	25113	74363
146672	2018-04-22	09:42:33	HSC-r2	63.2	50.7	2845	32509	18302	14207
161642	2019-01-07	15:31:21	HSC-g	57.4	55.0	358	40683	17182	23500
162680	2019-01-11	05:20:15	HSC-z	66.0	37.0	1874	33089	23908	9181
163754	2019-02-02	15:35:37	HSC-g	51.7	68.7	367	23441	16365	7076
190348	2019-11-01	10:00:11	HSC-g	60.7	61.1	418	26593	17657	8936
202364	2020-01-03	12:39:19	HSC-g	51.1	-67.2	396	24279	15839	8440
203690	2020-01-20	14:27:54	HSC-r2	67.3	-48.5	1017	27180	18166	9014

Table 3. Event information of the possible extensive air showers detected by Subaru HSC.
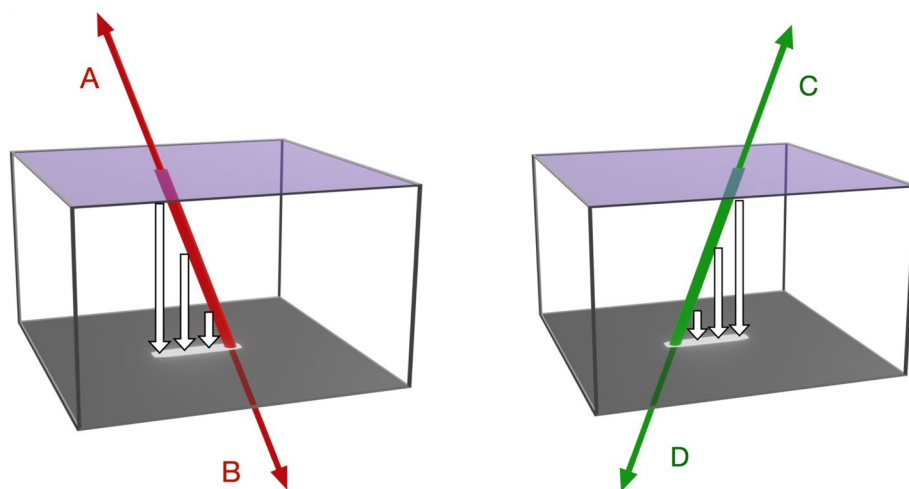

Figure 3. A schematic view of the four possible incident directions of a charged particle penetrating the depletion layer of a CCD. The open arrows indicate the direction of charge transfer inside the depletion layer of the CCD. All four incident directions result in the same track being recorded. The up-going directions (**A**) and (**C**) are unlikely for cosmic rays (and hence their associated secondary particles).

up-going particles are excluded (A and C in Fig. 3), then each measured track has two possible directions (B and D in Fig. 3). These directions differ by 180° in azimuth in the frame of the camera and have similar probabilities. For the sake of demonstration, we choose the trajectory with the smallest zenith angle. Regardless of whether this is the true direction, the observation of clustering will be evidence of an EAS. Choosing one direction in this way limits the effective detection area of the telescope to π sr.

For each visit, the directions of the detected tracks were traced back to their position on the sky and plotted as 2D histograms. Two example histograms for visits 073808 and 161642, together with the positions of the raw tracks on the CCDs, are shown in Fig. 4. The sky-map histograms have been divided into 12,288 bins, with each bin equivalent to ~ 0.001 sr. A clustering of particle arrival directions is clearly visible for both visits, indicating a common source for these particles i.e. a primary cosmic ray. All significant visits show some level of clustering. The open black circles in Fig. 4 represent the telescope pointing direction, with these regions also containing a large number of entries. This is due to both the increased likelihood of detecting particles coming from the telescope pointing detection and an artifact of the analysis procedure which causes the track detection algorithm to misinterpret stars, tracks which cross each other, and coincidental bundles of high signal pixels as short particle tracks.

Discussion and future objectives

For a single detector, the clustering observed in our results is encouraging and is evidence of having observed EASs. With additional silicon imaging detectors, the arrival direction, energy and mass composition of primary cosmic rays may be able to be reconstructed. Particle densities at each detector could be directly calculated based on the number of tracks and related to a primary energy through a lateral distribution fit, whilst the clustering
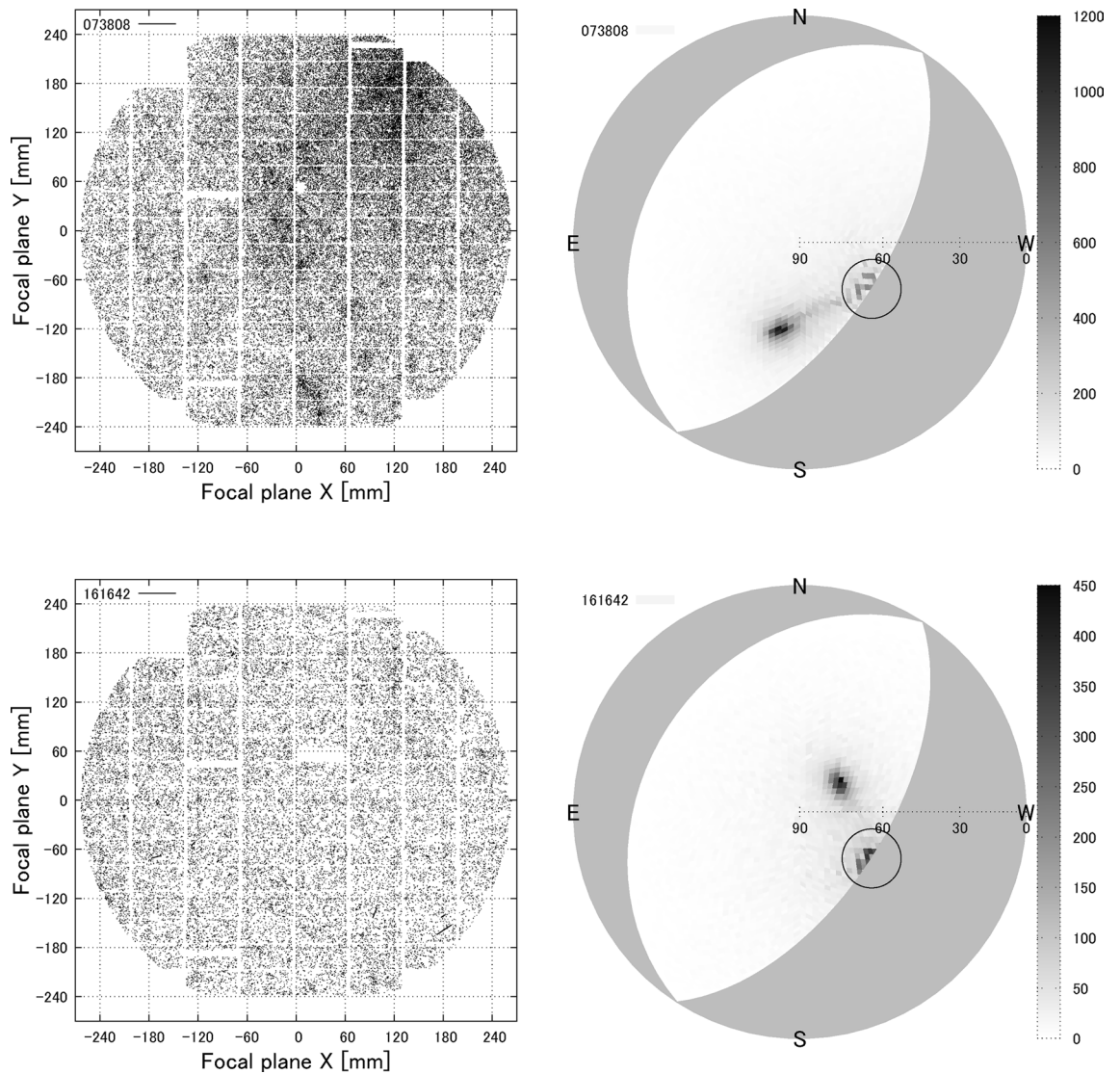
Figure 4. Arrival direction analysis for the largest and second largest excess visits of Subaru HSC. (Left) Positions of the secondary particle tracks in the CCDs. (Right) The traced back directions of the secondary particles in horizontal coordinates. The large open circles indicate the pointing direction of the telescope.

of secondary particle trajectories from *multiple* detectors could lead to a reconstruction of the arrival direction. Assuming we are able to distinguish electrons/positrons from muons, which could be accomplished by separating curved (electron/positron) and straight (muon) tracks, mass composition information on an event-by-event basis may also be accessible through calculating the electromagnetic-muonic component ratio of EASs.

Ultimately, we envision using silicon imaging detectors like Subaru HSC in conjunction with a SD array for highly detailed studies of EASs. With such a setup, the silicon imaging detector's ability to study EAS particle interactions in detail and determine event-by-event mass composition information could be combined with the precise knowledge of a showers energy and arrival detection from the SD array. We intend to test this concept by installing plastic scintillators inside the Subaru HSC building. This will allow us to look for coincident events between the two detectors.

Moving forward, we intend to cross-check the results in Table 3 with other telescopes at Maunakea Observatory, looking for time-coincident excesses evident of an EAS. If present, the particle densities at the different locations could be compared, similar to a SD array as described above, leading to a reconstruction of the primary energy. Possible future interdisciplinary applications include using detailed measurements of the vertex of muon decay inside the CCDs for searches of lepton flavor violating interactions such as $\mu^+ \rightarrow e^+ + e^- + e^+$, similar to the Mu3e experiment[18], and exotic signal searches for super heavy dark matter[19].

Conclusion

We have reported on the first results of detecting cosmic-ray extensive air showers with Subaru Hyper Suprime-Cam. Visits with a significant excess of secondary particle tracks in the CCDs were found and analysed for clustering of particle arrival directions. All visits displayed such clustering, indicating a single high-energy cosmic

ray origin for these particles. Additional measurements in conjunction with a SD array and collaboration with other observatories will be critical for taking full advantage of the unique properties of silicon imaging detectors as a tool for measuring extensive air showers.

Data availability
The data-sets used and/or analysed during the current study are available from the corresponding authors upon reasonable request.

References
1. Hess, V. F. Über Beobachtungen der durchdringenden Strahlung bei sieben Freiballonfahrten. *Phys. Z.* **13**, 1084–1091 (1912).
2. Alves Batista, R. *et al.* Open questions in cosmic-ray research at ultrahigh energies. *Front. Astron. Space Sci.* **6**, 23 (2019).
3. Coleman, A. *et al.* Ultra high energy cosmic rays the intersection of the cosmic and energy frontiers. *Astropart. Phys.* **147**, 102794 (2023).
4. Tokuno, H. *et al.* New air fluorescence detectors employed in the telescope array experiment. *Nucl. Instrum. Meth. A* **676**, 54–65 (2012).
5. Aab, A. *et al.* The pierre auger cosmic ray observatory. *Nucl. Instrum. Meth. A* **798**, 172–213 (2015).
6. Aab, A. *et al.* Measurement of the radiation energy in the radio signal of extensive air showers as a universal estimator of cosmic-ray energy. *Phys. Rev. Lett.* **116**, 241101 (2016).
7. Buitink, S. *et al.* A large light-mass component of cosmic rays at 1017–1017.5 eV from radio observations. *Nature* **531**, 70 (2016).
8. Schröder, F. G. Radio detection of cosmic-ray air showers and high-energy neutrinos. *Prog. Part. Nucl. Phys.* **93**, 1–68 (2017).
9. Abu-Zayyad, T. *et al.* The surface detector array of the telescope array experiment. *Nucl. Instrum. Meth.* **A689**, 87–97 (2012).
10. Abbasi, R. *et al.* Surface detectors of the TAx4 experiment. *Nucl. Instrum. Meth.* **1019**, 165726 (2021).
11. Aab, A. *et al.* Muons in air showers at the pierre auger observatory: mean number in highly inclined events. *Phys. Rev. D* **91**, 032003 (2015).
12. Arteaga Velazquez, J. C. A report by the WHISP working group on the combined analysis of muon data at cosmic-ray energies above 1 PeV. *PoS* **ICRC2023**, 466 (2023).
13. Miyazaki, S. *et al.* Hyper Suprime-Cam: System design and verification of image quality. *Publ. Astron. Soc. Jpn.* https://doi.org/10.1093/pasj/psx063 *(2018)*.
14. Johnson, T. H. & Street, J. C. The variation of the cosmic-ray intensity with azimuth. *Phys. Rev.* **41**, 690–690. https://doi.org/10.1103/PhysRev.41.690 (1932).
15. Johnson, T. H. Comparison of the angular distributions of the cosmic radiation at elevations 6280 ft. and 620 ft. *Phys. Rev.* **43**, 307–310. https://doi.org/10.1103/PhysRev.43.307 (1933).
16. Johnson, T. H. Progress of the directional survey of cosmic-ray intensities and its application to the analysis of the primary cosmic radiation. *Phys. Rev.* **48**, 287–299. https://doi.org/10.1103/PhysRev.48.287 (1935).
17. Bosch, J. *et al.* The Hyper Suprime-Cam software pipeline. *Publ. Astron. Soc. Jpn.* https://doi.org/10.1093/pasj/psx080 *(2018)*.
18. Arndt, K. *et al.* Technical design of the phase I Mu3e experiment. *Nucl. Instrum. Meth. A* **1014**, 165679 (2021).
19. Chung, D. J. H., Kolb, E. W. & Riotto, A. Superheavy dark matter. *Phys. Rev. D* **59**, 023501. https://doi.org/10.1103/PhysRevD.59.023501 (1998).

Acknowledgements

Author contributions
S.K. and M.K. identified the cosmic-ray air shower events with Subaru HSC and performed data analyses. T.F. and F.B. wrote the main part of the manuscript. S.M., Y.K., T.M., H.M., M.O. and T.T. meet the journal's authorship criteria for significant contributions to the detector construction, deployment, long-term data-taking and maintenance, software development and review of the manuscript.

Competing interests
The authors declare no competing interests.

Additional information
Correspondence and requests for materials should be addressed to S.K., M.K. or T.F.

Reprints and permissions information is available at www.nature.com/reprints.

Publisher's note Springer Nature remains neutral with regard to jurisdictional claims in published maps and institutional affiliations.